DOI: 10.61782/fa.2023.0318

forum acusticum 2023

Comparing predicted and observed strength and diffraction parameters for characterizing transmissions through a fluctuating water body

Jan Sliwka [1*] **Tommaso Fabbri** [1]

[1] NATO STO-Centre for Maritime Research and Experimentation (CMRE), Viale San Bartolomeo 400, La Spezia (SP), 19126, Italy.

ABSTRACT

This paper shows a comparison of observed and estimated strength and diffraction parameters in the context of acoustic transmissions through a fluctuating water body. These acoustic parameters characterize the saturation of an acoustic channel. The analysis is conducted on the dataset collected during the Mediterranean Rapid Environmental Picture (MREP) 20 sea trial held in the southern Mediterranean Sea in 2020. The prediction is based on applying path integral theory (work of S. M. Flatte and J. A. Colosi) using CTD data collected using a Wirewalker. A Wirewalker is a type of wave powered mooring able to continuously cast the water column with a high vertical resolution and provides the data to the user in real-time through telemetry. This makes it a powerful tool to observe oceanographic fine structure and more particularly internal waves and spice. The observations of these parameters is made through the analysis of acoustic data concurrently acquired during this sea trial. Specifically, the acoustic parameters are derived from the fluctuations in time of arrival and intensity of the received acoustic signals corresponding to a single consistent ray. The comparison shows coherence between the estimated and observed strength and diffraction acoustic parameters demonstrating the validity of the Wirewalker platform as a useful asset to estimate acoustic propagation regimes from oceanographic measurements.

[*] ***Corresponding author***: jan.sliwka@cmre.nato.int

Keywords: *Wirewalker, Channel saturation, Strength parameter, Diffraction parameter, Path integral theory.*

1. INTRODUCTION

The performance of underwater acoustic systems (e.g. sonar systems or underwater acoustic communication or navigation) depend heavily on the oceanic environment. In the effort of linking oceanography with acoustic performance, this work analyzes the impact of oceanographic fine structures on acoustic propagation in a shallow water environment. More specifically, this work focuses on the impact of sound speed fluctuations generated from diffuse internal-wave vertical displacement (waves fitting the Garrett-Munk spectrum). Similarly to surface waves, internal waves occur underwater between layers of different density of a stratified sea or ocean. They are usually characterized by a higher amplitude and longer wavelengths and can interfere with the acoustic waves that crosses it. More precisely, following the path-integral theory [1-2], the impact of oceanographic fine structures for a given acoustic channel can be described by the strength and diffraction parameters. The diffraction parameter, denoted as Λ, characterizes the diffraction effect caused by the sound-speed fluctuations of a given spatial extent. On the other hand, the strength parameter, denoted as Φ, is the root-mean-square (RMS) variation in an integral of the sound-speed fluctuations along the acoustic ray connecting the source and the receiver. Φ represents the RMS phase fluctuations of the received signal. Combining both parameters allows to determine the acoustic propagation regimes between unsaturated (weak scattering) and saturated (strong scattering). The more saturated the channel the worse is the quality of service for an acoustic

based system. The strength and diffraction parameters have been handled extensively in [1-2]. In these works, these parameters are estimated in acoustic channel setups characterized by long range propagation (hundreds of km) and a deep ocean with a sound channel guiding the acoustic waves. Application of this theory for experimental estimation of Λ-Φ parameters can be found in [3-7]. This paper deals with experimental validation of the path integral theory in shallower environment (experimental areas with bottom depth below in the order of few hundred meters) and short range transmissions (below 20 km). This is not the usual context of application of the equations covered by the literature and there are only few references which handle the modelling of such an environment [8]. The main difference with the deep water scenario is the interaction between the acoustic wave and the top and bottom interfaces. The analysis is performed on the data collected during the MREP20 experimentation held in the southern Mediterranean Sea in 2020. During this campaign, the equipment deployed included moorings with oceanographic and acoustic instruments, representing a good dataset for the development of the proposed framework. One of the highlights of the trial was the deployment of two Wirewalker platforms. This is a type of wave powered instrument (deployed in a moored or drifting mode) able to continuously cast the water column and therefore track the evolution of oceanographic features with a good spatial and temporal resolution. Furthermore, the capability of providing the sampled data directly to the user makes this platform suitable for operative scenarios in which a near real time analysis represent an added value. To recapitulate, the path integral theory is applied to predict the acoustic propagation regimes (saturated, partially saturated and unsaturated) starting from oceanographic measurements as provided by the Wirewalker and ship CTD data. These predictions are then validated based on acoustic data analysis of a transmission between a pair of transmitter-receiver.

The paper is organized as follows. Section 2 gives an overview of the MREP20 sea trial focusing on the assets considered in this study. Section 3 goes through the oceanographic data collected by the Wirewalker deployed during MREP20. The path integral theory used to estimate the strength and diffraction parameters is explained in Section 4. The algorithms used to estimate the strength and diffraction parameters from acoustic data are described in Section 5. In Section 6, the results from both approaches are compared. Finally, Section 7 draws the main conclusions.

2. MREP20 SEA TRIAL

The MREP20 experiment was a multi-institutional effort executed in Mediterranean Sea with the primary goal of investigating oceanographic variability at meso- and submeso-scales in the local Mediterranean environment and to assess its impact of different oceanographic processes on the acoustic propagation [9-10]. The MREP20 was conducted by NRV Alliance between the 27th of October and the 8th of November 2020 in an area south-east of Malta. The area was selected due to its complex dynamics generated by contribution of modified Atlantic and eastern Mediterranean waters. Of relevance on this experiment was the deployment of two Wirewalker (WW) units to cast continuously the water-column. Additional oceanographic/acoustic moorings equipped with hydrophones, acoustic sources and oceanographic sensors were also deployed.

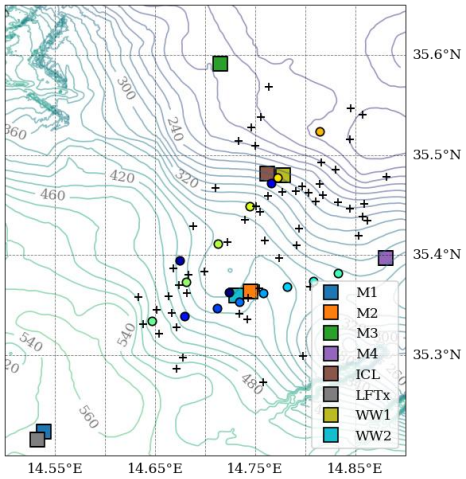

Figure 1. MREP20 map of the locations of the deployed moorings, as square markers, CTD casts, as circle markers and XBT casts as cross markers, executed during the entire experimentation.

In this work, the selected moorings of interest are the ones defining the acoustic channel considered. First, the M4 mooring equipped with a wide-band acoustic source, at ≈128 m depth representing the transmitter. Second, the M2 mooring equipped with a 4 element hydrophone array at the depth of approximately 92 m from which a single hydrophone is selected, representing the receiver of the selected acoustic channel. Additionally, WW2 moored next to M2 represents the mean to characterize the oceanographic environment. For completeness, Fig. 1

shows the spatial configuration of the set of oceanographic/acoustic moorings/platforms deployed as well as the ship CTD/XBT casts performed during the MREP20 experimentation.

3. OBSERVED SOUND SPEED FLUCTUATIONS

The variations of sound speed field strongly contributes to the acoustic variability. Such variations are due to a wide variety of oceanic processes such as shelf eddies or internal tides and waves. In this work, our attention is on sound speed fluctuations generated by diffuse internal-wave. These waves cause sound-speed fluctuations that can strongly limit the effectiveness of acoustic systems such as underwater communication or navigation. To have a complete characterization of the underwater field, and an assessment of the sound speed fluctuations, we considered the data collected through WW2. This platform was deployed in its moored configuration in an area characterized by a bathymetry of approx. 380 m, in the vicinity of the M2 mooring (the receiver of the acoustic channel considered). WW2 sampled the shallower 200 m of water column between the 30th of October and the 2nd of November 2020 with an average up-cast period of 20 min. with approximately 280 up-casts executed. Fig. 2 shows the binned and interpolated sound speed field derived from WW2 CTD up-cast measurements. The resulting field is characterized by a vertical resolution of 0.2 m and 20 min temporal resolution. Superimposed as black isolines, the tracked isopycnals (surface at constant density). Relevant to ocean acoustics is the mean vertical structure of the sound speed fluctuations $\langle \delta c(z) \rangle$. This is obtained empirically from the WW2 at each depth bin over the specific time window.

As highlighted in Fig. 3 the WW2 was not covering the whole water-column. To cover the deeper depth band, sound speed fluctuations can be expressed as function of the potential sound speed gradient, $(dc(z)/dz)_p$, and internal wave displacement ζ, as follows:

$$\langle \delta c^2(z) \rangle = \langle \zeta^2 \rangle \left(\frac{dc(z)}{dz} \right)_p^2 = \zeta_0^2 \frac{N_0}{N(z)} \left(\frac{dc(z)}{dz} \right)_p^2 \quad (1)$$

where the Wentzel-Kramers-Brillouin (WKB) has been used for the internal-wave displacement [11]. Also, $N(z)$ is the buoyancy frequency profile, N_0 is the surface extrapolated buoyancy frequency and ζ_0 is the

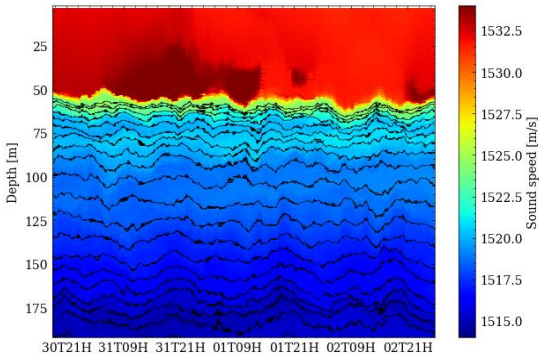

Figure 2. Sound speed field binned and interpolated in the time and depth domain using up-casts collected through WW2. Superimposed in black, the contour lines of the tracked isopycnals.

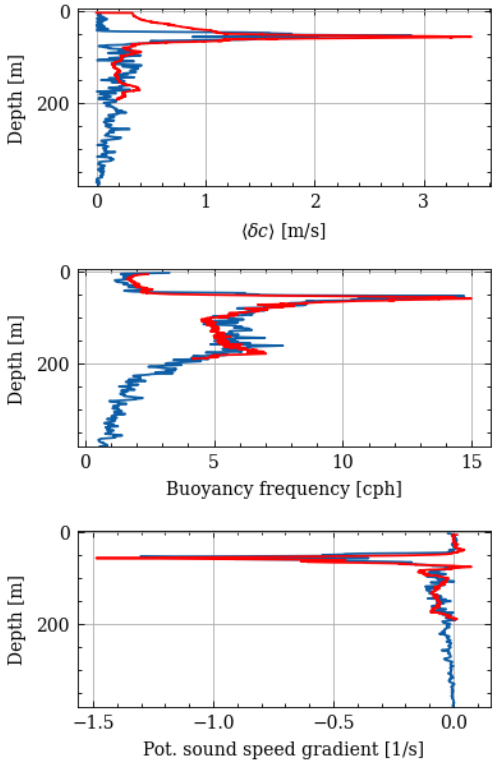

Figure 3. Profiles of sound speed fluctuations (top), buoyancy frequency (middle) and potential sound speed gradient (bottom). The profiles were derived from CTD casts, in blue color, and empirically from WW2 measurements in red color for the time window considered.

displacement of an the isodensity surface where $N = N_0$. Through the above relation, the RMS displacement in the deeper depth band is estimated through the CTD casts executed from the NRV Alliance in the temporal window of interest. The value of $\zeta_0^2 N_0 = 0.02\mathrm{m}^2\mathrm{rad/s}$ has been estimated through the minimization of the difference between the observed values of $\langle \delta c^2(z) \rangle$ from the Wirewalker measurements with the ones estimated through the WKB approximation in the top 200m.

4. ESTIMATION OF Λ - Φ USING PATH INTEGRAL THEORY

This section collects the main equations for the calculation of Λ - Φ parameters. The equations are from the reference books [1-2] and more recent papers.

4.1 Strength parameter Φ

The strength parameter Φ is the RMS variation in phase of a signal at the receiver under the geometrical optics approximations. In our implementation, we refer to the formulation for the mean square phase parameter Φ^2 described in [12]. This quantity is estimated along each eigen-ray Γ connecting the source with the receiver for the selected acoustic channel setup. The formula used in this paper is

$$\Phi^2 = \omega_c^2 \int_\Gamma \mathrm{d}s \frac{1}{c_b^4(z)} \langle \delta c^2(z) \rangle L_P(\theta, z) \qquad (2)$$

where $c_b(z)$ is the background sound speed (or equilibrium sound channel) and $\delta c(\boldsymbol{x}, t)$, the perturbation due to internal waves, ω_c^2 is the angular frequency of the transmitted signal, $L_P(\theta, z)$ is the correlation length of the sound fluctuations along the direction of the ray, θ and for a given depth z. It is worth mentioning that $\theta(s)$ and $z(s)$ are functions of the ray path, Γ, but its argument has been removed in the equations for readability.

4.2 Diffraction parameter Λ

The diffraction parameter Λ characterizes the diffraction effect caused by the sound-speed fluctuations of a given spatial extent. Using the formulation from [12] the diffraction parameter is formulated as follows:

$$\Lambda = \frac{\omega_c^2}{\Phi^2} \int_\Gamma \mathrm{d}s \frac{\langle \delta c^2(z) \rangle L_p(\theta, z)}{c_b^4(z)} \frac{\{m^2\} R_f^2(x)}{2\pi} \qquad (3)$$

where $R_f^2(x)$ represents the extension of the vertical Fresnel zone radius along the selected ray, and $\{m^2\}$ is the vertical wavenumber of the medium sound-speed fluctuations, and the curly brackets indicate an average over the spectrum with the perpendicular wavenumber constraint. For details about the quantities $R_f^2(x)$ and $\{m^2\}$ we refer to the approximated formulas provided in [2-3].

4.3 Estimation Procedure

The estimation of the Λ-Φ parameters is performed for several consecutive temporal windows of different size covering 6, 12 and 24 hours. For each window, the background sound speed profile as well as the empirical sound speed fluctuations and the required oceanographic parameters are computed. Next, the eigen rays (acoustic rays/paths linking the transmitter with the receiver) are estimated using the Bellhop model [13] for the selected acoustic channel geometry. This is defined through the depths of the transmitter and receiver, the range separating the two ends, the associated bathymetry and finally the background sound speed profile for the temporal window considered. In this work, among all the rays provided by the model, we considered the most energetic rays (which are also the ones characterized with limited interactions with the boundaries), for the Λ-Φ calculations. Fig. 4, as an example, shows the resulting eigen rays connecting transmitter and receiver as estimated through the Bellhop model for a mean profile for a single window covering 6 hours. For each ray, a Λ-Φ estimate is calculated and the final result is presented in the form of the mean and standard deviation of all estimates. The reason is to grasp the overall picture with regards to the saturation of the channel and account for simulation imprecisions (such as assuming a constant sound speed profile).

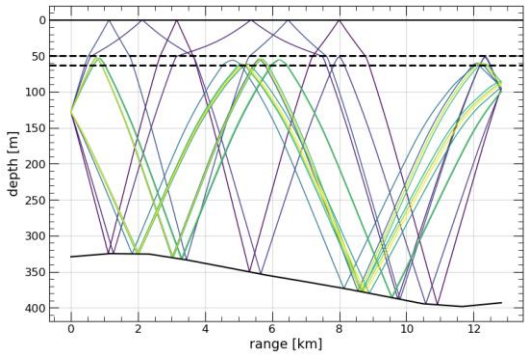

Figure 4. Eigen rays calculated using the Bellhop model for a single window of 6 hours. The two dashed lines delimit the area with the highest sound speed fluctuations.

5. CALCULATION OF Λ-Φ FROM ACOUSTIC DATA

5.1 Equations

Experimentally, the strength parameter Φ can be obtained using the following formula defined in [11], here reported:

$$\Phi = 2\pi f \sigma_t \tag{4}$$

where σ_t is the standard deviation of the time of arrival of a wave of frequency f.

The scintillation index (SI) is obtained using the following equation defined in [2]:

$$\mathrm{SI} = \frac{\mathrm{E}\{\mathrm{I}^2\} - \mathrm{E}^2\{\mathrm{I}\}}{\mathrm{E}^2\{\mathrm{I}\}} = \frac{\mathrm{VAR}\{\mathrm{I}\}}{\mathrm{E}^2\{\mathrm{I}\}} \tag{5}$$

where I is the intensity of the incoming acoustic wave (or a quantity proportional to the intensity since the SI is the normalized intensity variance).

Finally, the diffraction parameter Λ can be deducted using the following equation [1]:

$$\Lambda = \frac{4\mathrm{SI}}{\Phi^2} \tag{6}$$

It is worth to mention that this equation is only applicable when the acoustic channel is in the unsaturated regime. This is established by considering the estimates from the path integral theory based (from the formulation of the previous section).

5.2 Acoustic dataset

The source transmitted an LFM signal with frequencies ranging from 800 Hz to 12 kHz every 30 seconds. Because of the low sampling rate of the receiver (around 10 kHz) the LFM section considered for the analysis was $3000 \pm 500Hz$.

5.3 Acoustic processing

The signal is composed of a series of chirps repeated every fixed interval. This allows to compute a time varying channel impulse response. The output is a series of signal arrivals with varying amplitudes for each timestamp. These arrivals are then fed to the curve tracing algorithm to identify the curve consistently containing most of the strongest arrivals which is named overall-strongest. Curve tracing is necessary as the strongest arrivals are not always on the same curve. In this paper only single curve tracing is considered. The overall-strongest curve was one of the most complete curves and therefore reliable to track. Some of the other curves containing weaker arrivals have missing sections. Future work may involve simultaneous tracking of all arrivals in order to make an individual analysis on every single ray. The obtained curve is then compensated for the relative clock drift between the transmitter and receiver by setting the slope of the linear fit of the curve to zero. This result can then be used to estimate Φ and SI.

For estimating the strength parameter, Φ, a band pass filter is applied in order to filter out the tides K1 and M2 physically affecting the mooring as well as high frequencies which cannot be sampled by the Wirewalker (which samples the environment at a much slower rate). The standard deviation is then calculated for consecutive windows of a given size and Eqn. (4) is used to calculate Φ.

For the scintillation index, SI, the same band pass filter is applied to filter the tidal variations of the amplitude around the mean amplitude value. This method was used since the amplitudes are strictly positive. Eqn. (5) is then used to compute the SI for consecutive windows of a given size.

Fig.5 shows the result of the match filtering, peak detection and curve tracing. The raw output of the curve tracing algorithm is shown in red. The low pass filtered output of the curve tracing algorithm is shown in green and the low frequency component, which contains the tidal components, is shown in black. The latter curve highlights the high frequency fluctuations.

The tracker is based on a simple filter that at each time-stamp selects the best data point using a double-objective optimization. The selected arrival is a compromise between being the strongest arrival and being the closest to a predicted value based on the last N measurements. Considering t_p being the predicted time of arrival, t_i and w_i being respectively the arrival times and amplitudes at the current time-stamp, the selected arrival has to maximize this coefficient:

$$\frac{(1 + \alpha w_i)}{\left(1 + \beta\left(t_i - t_p\right)\right)^2} \tag{7}$$

where α and β are design constants. t_p is obtained extrapolating a linear fit of the last N filtered data points.

The fluctuations of the time of arrival filtered of the tidal contributions, used for the calculation of Φ, are shown in Fig. 6.

The fluctuation of the intensity filtered for the tidal contributions are shown in Fig. 7. The intensity has been normalized by its mean value (SI calculation is not affected by a multiplicative constant). Finally the scintillation index is calculated from Eqn. (5). The SI using a data window for the statistical analysis of 3 hours is shown in Fig. 8.

The resulting Λ-Φ parameters are shown in Section 6 where the comparison of estimated and observed parameters is being made.

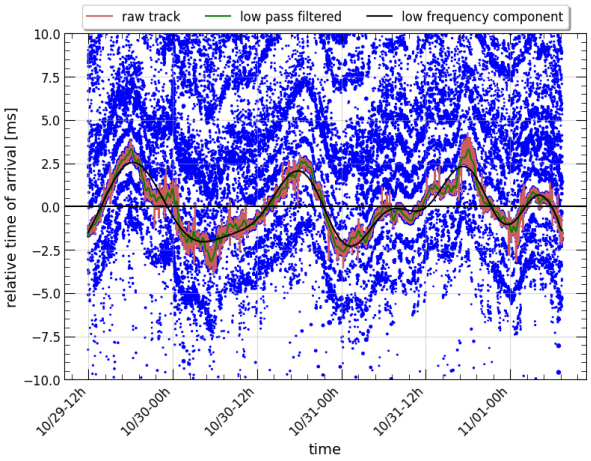

Figure 5. Results of the curve tracing algorithm to extract the consistently strongest arrival curve for the 3 kHz LFM section.

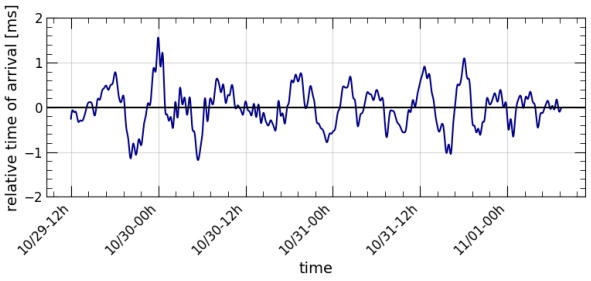

Figure 6. Fluctuations of the time of arrival filtered for the tide for the 3 kHz LFM section.

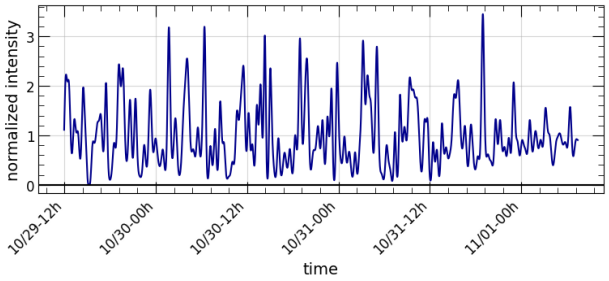

Figure 7. Fluctuations of the intensity filtered for the tide for the 3 kHz LFM section.

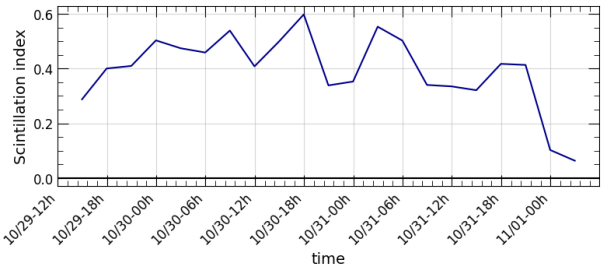

Figure 8. Scintillation index for the 3 kHz LFM section.

6. COMPARISON OF ESTIMATED AND OBSERVED VALUES

In this section the Λ-Φ parameters estimated using the path integral theory are compared to the values obtained using the acoustic processing. The overlap between acoustic recordings and Wirewalker data recordings covered multiple days.

Fig. 9 shows the comparison between the observed and estimated Φ considering different temporal window sizes: 6 hours in the top panel, 12 hours in the middle panel and 24 hours bottom panel. Note that the larger the analysis window the smoother the observed value of Φ. Overall, there is a good match between the observed and estimated values especially using the 24 hour window. The observed value of Φ does fluctuate with the tide, an effect which does not seem to be reproduced in the theoretical curve. More investigation is needed to understand this behavior.

Similarly, Fig. 10 shows the comparison between the observed and estimated Λ values, the observations are the same as in the case of Φ. The high fluctuations of Λ are a

direct consequence of the fluctuations of Φ since the latter is used to estimate Λ (as reported in Eqn. (3)).

The Λ-Φ parameters are usually plotted in a Λ-Φ diagram which allows for pinpointing the saturation regime. Fig. 11 shows the joint Λ-Φ plot for a window of 6h. The comparison shows consistency between observed and estimated acoustic parameters and that the regime is unsaturated bordering on partial saturation.

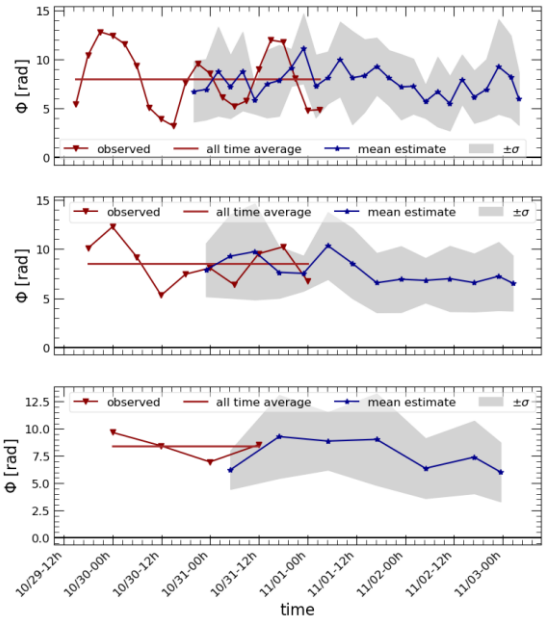

Figure 9. Comparison between the observed and estimated Φ for different window lengths.

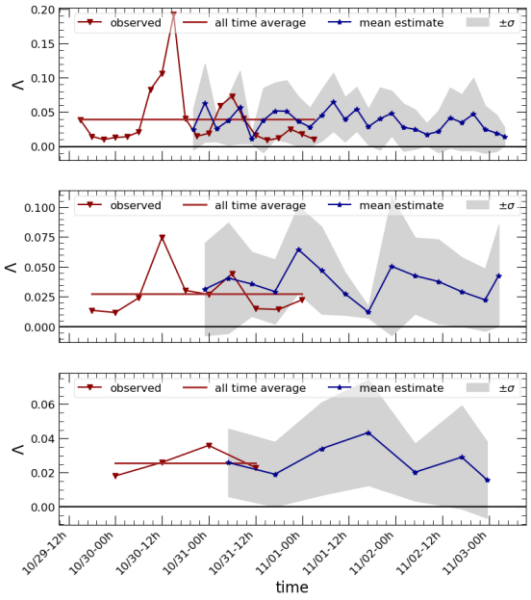

Figure 10. Comparison between the observed and estimated Λ for different window lengths.

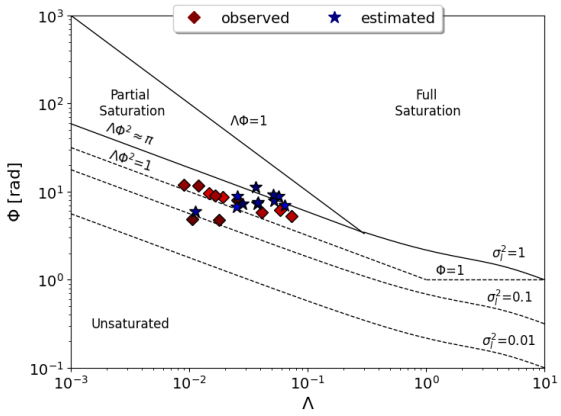

Figure 11. Λ-Φ plot for comparing the observed and estimated acoustic parameters for a window of 6 hours.

7. CONCLUSION

In this paper, Wirewalker data has been used to analyze the impact of oceanographic fine-structure on acoustic transmissions. The analysis of the Wirewalker data consisted in the calculation of the acoustic parameters characterizing the saturation of the acoustic channel namely

the strength and diffraction parameters. These parameters were obtained using path integral theory. The aim was to compare the theoretical values with the ones observed in the acoustic data collected concurrently with the Wirewalker data. The comparison showed consistency between observed and estimated acoustic parameters and shows that the approach is promising even in shallow waters and for short range transmissions. The results also shows that the choice of the analysis window is an important factor to consider when observing the acoustic parameters. However, the all-time average value is consistent for all values of the window length. The results for the theoretical estimates may be improved by extending the sampling of the depth column to better capture the fluctuations below 200m. The results of the acoustic processing may be improved by using arrays of hydrophones and use array processing to better differentiate between the different arrivals / rays. Also, as mentioned earlier, a simultaneous tracking of all arrivals can be implemented for an extended analysis. This paper has shown that one of the advantage of using ray path integral theory is that the strength and diffraction parameters can be calculated using only oceanographic measurements. In fact, the observation of the strength parameter Φ for a short range scenario requires a high precision of measurement and tracking of the time of arrival as well as a stable TX and RX platforms and a good clock synchronization. This is usually hard to achieve experimentally, especially when the transmitter platform is mobile (Ship-borne transmitter).

8. REFERENCES

[1] R. Dashen, W. H. Munk, K. M. Watson and F. Zachariasen, Sound transmission through fluctuating ocean, S. M. Flatté, Ed., Cambridge University Press, 1980.

[2] J. A. Colosi, Sound Propagation through the Stochastic Ocean, Cambridge University Press, 2016.

[3] J. A. Colosi, "A reformulation of the $\Lambda-\Phi$ diagram for the prediction of ocean acoustic fluctuation regimes," *The Journal of the Acoustical Society of America* , vol. 137, no. 5, 2015.

[4] R. Esswein and S. M. Flatté, "Calculation of the strength and diffraction parameters in oceanic sound transmission," *The Journal of the Acoustical Society of America,* vol. 67, no. 5, 1980.

[5] M. D. Vera, "Comparison of ocean-acoustic horizontal coherence predicted by path-integral approximations and parabolic-equation simulation results," *The Journal of the Acoustical Society of America,* vol. 121, 2007.

[6] S. M. Flatté and G. Rovner, "Calculations of internal-wave-induced fluctuations in ocean-acoustic propagation," *The Journal of the Acoustical Society of America,* vol. 108, no. 2, 2000.

[7] R. K. Andrew and A. Ganse, "Low-frequency pulse propagation over 510 km in the Philippine Sea: A comparison of observed and theoretical pulse spreading," *The Journal of the Acoustical Society of America,* vol. 140, 2016.

[8] J. A. Colosi, T. F. Duda and A. K. Morozov, "Statistics of low-frequency normal-mode amplitudes in an ocean with random sound-speed perturbations: Shallow-water environments," *The Journal of the Acoustical Society of America,* vol. 131, 2012.

[9] P.-M. Poulain and P. Oddo, "Cruise report and datasets during the MREP20 sea trial," no. CMRE Technical Progress Report A06.4.2.1, 2020.

[10] P.-M. Poulain, P. Oddo, G. Pennucci, C. Lewis, J. Sliwka, T. F. Duda and A. Drago, "Observations of internal tidal dynamics Southwest of Malta in the central Mediterranean Sea," *Continental Shelf Research,* vol. 254, 2023.

[11] J. A. Colosi, E. K. Scheer, S. M. Flatté, B. D. Cornuelle, M. A. Dzieciuch, W. H. Munk, P. F. Worcester, B. M. Howe, J. A. Mercer, R. C. Spindel and others, "Comparisons of measured and predicted acoustic fluctuations for a 3250-km propagation experiment in the eastern North Pacific Ocean," *The Journal of the Acoustical Society of America,* vol. 105, pp. 3202-3218, 1999.

[12] J. A. Colosi, B. D. Cornuelle, M. A. Dzieciuch, P. F. Worcester and T. K. Chandrayadula, "Observations of phase and intensity fluctuations for low-frequency, long-range transmissions in the Philippine Sea and comparisons to path-integral theory," *The Journal of the Acoustical Society of America,* vol. 146, pp. 567-585, 2019.

[13] M. Porter, "The bellhop manual and user's guide: Preliminary draft," 2011.